Zhao Jiuwei (Orcid ID: 0000-0001-9146-7500)
Zhan Ruifen (Orcid ID: 0000-0001-7209-0904)
Wang Yuqing (Orcid ID: 0000-0002-1691-8161)

Different responses of tropical cyclone tracks over the western North Pacific and North Atlantic to two distinct SST warming patterns

Jiuwei Zhao[1,2,4], Ruifen Zhan[1,2*] and Yuqing Wang[3,2]

[1]Department of Atmospheric and Oceanic Sciences & Institute of Atmospheric Science, Fudan University, Shanghai, China

[2]State Key Laboratory of Severe Weather, Chinese Academy of Meteorological Sciences, Beijing, China

[3]International Pacific Research Center and Department of Atmospheric Sciences, School of Ocean and Earth Science and Technology, University of Hawaii at Manoa, Honolulu, Hawaii, USA

[4]Key Laboratory of Meteorological Disaster, Ministry of Education (KLME), Nanjing University of Information Science & Technology (NUSIT), Nanjing, China

December 31, 2019 (submitted)
February 10, 2020 (first revision)
March 2, 2020 (second revision)

Dateline

Key points

1) The La Niña-like warming reduces (increases) TC track density in the main WNP (NA), while the El Niño-like warming reduces it in two basins.
2) The different responses are due to the different tropical zonal SST gradients associated with the two warming patterns.
3) China and North America would experience more landfalling TCs in La Niña-like warming pattern than in El Niño-like warming pattern.

Submitted to ***Geophysical Research Letters***

**Corresponding author address*:
Prof. Ruifen Zhan
Department of Atmospheric and Oceanic Sciences &
Institute of Atmospheric Science, Fudan University.
2005 Songhu Road, Shanghai, 200438, China.

This article has been accepted for publication and undergone full peer review but has not been through the copyediting, typesetting, pagination and proofreading process which may lead to differences between this version and the Version of Record. Please cite this article as doi: 10.1029/2019GL086923

©2020 American Geophysical Union. All rights reserved.

Email: zhanrf@fudan.edu.cn

ABSTRACT

How future tropical cyclone (TC) activity could change under global warming (GW) is enormously important to society, which has been widely assessed using state-of-the-art climate models. However, these models were predominantly based on projection of an El Niño-like warming pattern. Recent studies suggested that a La Niña-like warming pattern is also possible. Here, we compare the responses of TC track density (TCTD) over the western North Pacific (WNP) and North Atlantic (NA) to the two distinct GW patterns. We find that the La Niña-like warming pattern reduces WNP TCTD except in the South China Sea and along China coast and increases NA TCTD, while the El Niño-like warming pattern generally reduces TCTD in both basins. This is due to different responses of large-scale dynamic/thermodynamic conditions to the distinct zonal sea surface temperature gradients associated with the two warming patterns. These results help better understand potential future change in TC tracks.

Accepted Article

©2020 American Geophysical Union. All rights reserved.

1. Introduction

How future tropical cyclone (TC) activity could change under global warming (GW) has received increasing attention owing to its potential devastating impacts on our society. Particularly, future change in TC genesis and tracks is extremely important because it is directly associated with TC landfall and societal impact. Two recent examples of landfalling TCs are Hurricane Sandy in 2012 and Typhoon Haiyan in 2013 that caused massive damage to the U.S. and the Philippines, respectively (e.g., Blake et al. 2013; Schiermeier, 2013).

State-of-the-art climate models have been widely used in examining the responses of TC activity to GW and the involved physical mechanisms (Knutson et al., 2019, 2020; Walsh et al., 2016). The majority of climate models projected an eastward shift from the western North Pacific (WNP) toward the central North Pacific and from the western North Atlantic (NA) to the eastern NA for TC track density (TCTD) under a warmer climate, with decreasing TCTD over the WNP and the western NA (Colbert et al., 2013; Li et al., 2010; Murakami et al., 2011; Murakami et al. 2012; Nakamura et al., 2017), although some studies suggested a pronounced increase over the WNP (Emanuel, 2013; Park et al., 2017). Several previous studies suggested a significant decrease in westward moving TCs and an increase in recurving TCs over the WNP (Colbert et al., 2015; Yokoi et al., 2013) and the NA (Colbert et al., 2013; Murakami & Wang, 2010). The track shift is generally attributed to changes in the large-scale steering flow and the shift of TC genesis location, which are primarily associated with a weakening of the mean atmospheric circulation in response to GW (Colbert et al., 2013; Wu & Wang, 2004).

Most previous studies on the projected future TC changes are mainly based on sea surface temperature (SST) forcing that has an El Niño-like warming pattern with relatively faster warming over the central and eastern tropical Pacific derived from the third or fifth Coupled Model Intercomparison Project (CMIP3 or CMIP5) models (Cai et al., 2015; Chen et al., 2017; Taylor et al., 2012; Vecchi et al., 2006; Zhang & Wang, 2017; Zhang & Li, 2014).

©2020 American Geophysical Union. All rights reserved.

However, it is well known that the coupled climate models have a cold tongue bias in the tropical Pacific, which could introduce considerable uncertainty in the projected future SST warming pattern (Luo et al., 2018; Seager et al., 2019). Recently, observational studies have shown a La Niña-like warming trend over the tropical Pacific in response to rising CO_2 in recent decades, with relatively slower warming over the central Pacific than over other tropical oceans (Kohyama et al., 2017; Lian et al., 2018; Luo et al., 2012, 2018; Seager et al., 2019). Since the projected TC activity can be sensitive to different SST patterns (Knutson et al., 2015; Murakami et al., 2012; Zhao et al., 2009), the La Niña-like SST warming pattern could lead to changes in the projected future TC activity quite different from the El Niño-like warming pattern. Therefore, it is an urgent issue to address how different the changes in the projected TC activity could be under the two distinct warming trends (Lian et al., 2018; Seager et al., 2019).

In this study, we compare the responses of TCTD over the WNP and NA to the abovementioned two distinct warming patterns based on the observed SST trend pattern and the multi-model ensemble projected SST pattern from 12 CMIP5 models under the Representative Concentration Pathway 8.5 (RCP8.5) scenario using the high-resolution atmospheric general circulation model (HIRAM-C180). We find that the projected future changes in TCTD exhibit pronounced differences in spatial distributions in response to the two distinct warming patterns. The La Niña-like warming pattern tends to reduce TCTD over the WNP except in the South China Sea and along China coast, but increase TCTD over the NA, while the El Niño-like warming pattern generally reduces TCTD in both basins. These findings can help better understand future change in TC tracks, and also call for attention to uncertainties in the projected future SST pattern when the impact of GW on TC activity is assessed.

Accepted Article

©2020 American Geophysical Union. All rights reserved.

2. Data and Methodology

2.1 Observational data

The observed monthly mean SST data were derived from the Extended Reconstructed SST version 4 (ERSST.V4) data during 1960–2014 from the National Oceanic and Atmospheric Administration (NOAA; Huang et al., 2015).

2.2 HIRAM model and experiments

The HIRAM-C180 was used to conduct numerical experiments to examine responses of TCTD over the WNP and NA to two different warming patterns in this study. The HIRAM-C180 was developed by the Geophysical Fluid Dynamics Laboratory (GFDL; Zhao et al., 2009), which has the horizontal grid spacing of roughly 50 km and 32 vertical levels. The dynamical core is discretized with the finite-volume method on a cubed-sphere grid topology. The related details can be found in Putman & Lin (2007). Previous studies have shown that the HIRAM-C180 can well reproduce the spatial distribution of the observed TC tracks (Zhao et al., 2009). Additionally, some studies have also demonstrated that the HIRAM-C180 can skillfully predict interannual variations in TC genesis frequency over the WNP and the NA (Murakami et al., 2011, 2016; Murakami & Wang, 2010).

The model was integrated from January 1990 to December 2009 for each run. The control (CTRL) experiment used the observed monthly mean SST as the boundary condition to produce present climate simulations. Two future runs were conducted by adding the SST warming patterns to the observed monthly mean SSTs (Sugi et al., 2015). One was driven by the La Niña-like warming pattern represented by the SST in the CTRL experiment plus the observed SST trend in the period 1960–2014 (Fig. 1a; GWLA run), and the other was driven by the El Niño-like warming pattern derived from the SST in the CTRL experiment plus the projected SST trend from the multi-model ensemble mean of 12 CMIP5 models (Supplementary Table S1) for the period 2006–2099 under the RCP8.5 scenario (Fig. 1b;

©2020 American Geophysical Union. All rights reserved.

GWEL run). The differences between GWLA (GWEL) and CTRL runs averaged over June-November during 1990–2009 were regarded as the response to the La Niña-like (El Niño-like) warming. Note that greenhouse gases concentrations in the study were derived from observations as used in the standard HIRAM-C180 model without any change in all runs. Also note that the SST warming pattern was added as a stationary global warming pattern without seasonal variation considered in all simulations. We selected the period 1960–2014 to derive the La Niña-like warming pattern from the observation because the impact of the interdecadal variability can be removed as much as possible in this period. The TC detection algorithm is described in Appendix. TCTD is defined as the TC occurrence frequency (TCOF) in each 5°×5° grid box. TCOF in a grid box is counted once if a named TC passed (appeared in) the box.

In addition to the GCM, the Lindzen-Nigam model (LN87; Lindzen & Nigam, 1987) was used to evaluate impacts of the SST gradients associated with the two warming patterns on the low-level atmospheric circulation. The model detail is also given in Appendix.

3. Results

Figure 1 shows the linear trend increments averaged over June–November (JJASON) from observations during 1960–2014 and from the ensemble mean of 12 CMIP5 model simulations during 2006–2099. In both cases, the SST shows a consistent warming, however, the warming trends in the Pacific Ocean are greatly different from each other. The observed SSTs (Fig. 1a) exhibit a clear La Niña-like warming pattern with slower warming in the central Pacific than in other tropical oceans, while the climate model ensemble mean SSTs (Fig. 1b) show an El Niño-like warming pattern with faster warming over the central and eastern tropical Pacific than over the western tropical Pacific. As a result, a sharp SST gradient exists between the tropical WNP and central Pacific in the former, while the SST gradient becomes relatively complicated in the latter. A similar result is obtained from the warming increment of ensemble

©2020 American Geophysical Union. All rights reserved.

mean SST during 2045–2099 (Supplementary Fig. S1), with the same time length as the observed SST during 1960–2014. This similarity suggests that the El Niño-like GW pattern is stable in describing future SST change derived from the CMIP5 ensemble mean. Another notable difference in the warming patterns between observation and model ensemble is the SST gradient between the central-eastern Pacific and the Atlantic. Compared with the central-eastern Pacific, the Atlantic has much larger warming increments in observation, while it turns to be relatively low in model ensemble. This different SST gradient may lead to a quite different circulation response over the NA to GW (Choi et al., 2019; Patricola et al., 2016). Note that the above two warming patterns from observation and model ensemble will be simply referred to as the La Niña-like and El Niño-like warming patterns, respectively, in the following discussion.

Figure 2 shows the simulated changes in TCTD over the WNP and NA forced by the two SST warming patterns, respectively. In comparison with observation, the CTRL run generally reproduced reasonably the climatology and interannual variability of TC genesis frequency (Supplementary Fig. S2) and TCTD (Supplementary Figs. S3 and S4). When the model is forced by the La Niña-like warming pattern, the simulated difference in WNP TCTD from the CTRL run shows a pronounced dipole distribution, with a significant decrease east of Philippines (including Japan and Korea) and an increase over the South China Sea (SCS), along China coast, and the Philippines (Fig. 2a), while the difference in NA TCTD is characterized by a nearly uniform increase except in some sporadic areas where the differences show an insignificant decrease (Fig. 2b). In sharp contrast, when the model is forced by the El Niño-like warming pattern, the changes in TCTD over both the WNP and the NA turn to a decrease in most regions despite a small increase on the edge of the WNP and east of the Caribbean Sea (Figs. 2c and 2d). The TC genesis frequency exhibits similar changes (Supplementary Fig. S5). Therefore, our results show that the responses of TCTD over both the WNP and the NA to the two warming patterns are pronouncedly different. In response to the El Niño-like warming

©2020 American Geophysical Union. All rights reserved.

pattern, TCTD is more likely to decrease in the main regions of both basins, while in response to the La Niña-like warming pattern, TCTD tends to decrease east of Philippines over the WNP but increase over the SCS, along China coast, and the Philippines and nearly increase uniformly over the NA.

To understand the different responses, we examined changes in the large-scale environment that are often believed to control TC activity in response to the La Niña-like and El Niño-like warming patterns (Fig. 3), including the low-level winds (LLW), sea level pressure (SLP), vertical zonal wind shear between 200 hPa and 850 hPa (VZWS), relative humidity (RH) at 600 hPa, and steering flow (SF) defined as the deep layer mass-weighted mean wind between 300 and 850 hPa. Among these, the mid-tropospheric RH is a thermodynamic factor, and others are large-scale atmospheric dynamical factors. In general, westerly anomalies over the tropics along with anomalous cyclonic circulation off the equator in the lower troposphere are favorable for TC genesis and development, while large-scale SF is essential for TC movement (Wu & Chen, 2016). The VZWS and the mid-level RH are negatively and positively correlated with TC activity, respectively.

In response to the La Niña-like warming pattern, significant easterly and positive SLP anomalies are present over the tropical WNP east of the Philippines and an anomalous cyclonic circulation and negative SLP anomalies are located from the SCS to the East China Sea, while significant westerly anomalies cover the tropical NA along with an anomalous cyclonic circulation and negative SLP anomalies off the equator over the NA (Fig. 3a). The changes in large-scale SF (Fig. 3c) are characterized by an anomalous cyclonic-anticyclonic dipole over the WNP with their centers over the SCS and east of Japan, respectively, and anomalous easterly over the coastal areas of America. The above responses in the wind and SLP fields are favorable for TC genesis and subsequent development over the SCS and the NA as well as favorable for TCs to make landfall over China and North America, but reduce TCTD over the

©2020 American Geophysical Union. All rights reserved.

WNP east of the Philippines. Moreover, the positive VZWS and negative RH anomalies over the main WNP also suppress TC genesis and reduce TCTD over the WNP east of the Philippines, while the negative VZWS and positive RH anomalies over the SCS and the NA enhance local TCTD (Figs. 3e and 3g).

In response to the El Niño-like warming pattern, the LLW anomalies show a zonal dipole structure over the North Pacific with cyclonic circulation anomalies over central-eastern North Pacific and anticyclonic anomalies over the WNP, and a meridional dipole over the NA with an anomalous anticyclonic circulation over the tropical NA and an anomalous cyclonic circulation over the subtropical NA (Fig. 3b). The SLP and VZWS exhibit an increase in the major TC active regions of the WNP and NA but a decrease over the central Pacific (Figs. 3b and 3f). These dynamical conditions in response to the El Niño-like warming are consistent over both the WNP and the NA, and less favorable for TCTD over both basins. Note that the increase in TCTD over the middle SCS and the coastal area of North America is likely to be associated with the anomalous westward SF (Fig. 3d). Unlike the local dynamical conditions, the RH over the NA shows an overall increase (Fig. 3h), which coincides with the strong warming in the equatorial Atlantic (Fig 1b) and could be explained by the warmer-get-wetter mechanism in the tropical oceans (Xie et al. 2010). This increase seems to be favorable for TCTD over the NA, and may partly explain the relatively small decrease in TCTD over the NA in response to the El Niño-like warming (Fig. 2d).

Previous studies have shown that small changes in SST and SST gradient can lead to shift in the location of large-scale organized convection in the tropics, resulting in large anomalies in atmospheric circulation from the tropics to the extratropics (Trenberth et al., 1998). It is our interest to further examine how the local large-scale dynamic and thermodynamic conditions change in response to the two distinct warming SST patterns (Fig. 1). Figure 4 compares the changes in the velocity potential and the associated divergent wind at 850 hPa

©2020 American Geophysical Union. All rights reserved.

and 200 hPa, and surface precipitation in response to the La Niña-like and El Niño-like warming patterns. The 200-hPa velocity potential consistently shows a dominant wavenumber-3 structure in response to the two warming patterns (Figs. 4c and 4d). A large phase shift in the wave-like structure is evident between the two responses. The large increase in the upper-level velocity potential centered over the Indian Ocean in response to the La Niña-like warming pattern shifts to the East Indian Ocean–western Pacific and even becomes much stronger in response to the El Niño-like warming pattern, indicating that the WNP changes from ascending to sinking anomalies. It is also evident that in response to the El Niño-like warming pattern the strong positive upper-level velocity potential center over the central Pacific does not appear and the weak negative center over the equatorial eastern Pacific becomes stronger than that in response to the La Niña-like warming pattern. This leads to a substantial change in the Walker circulation across the tropical Pacific, changing from the ascending anomaly over the WNP and the descending anomaly over the Indian Ocean and the central Pacific to the sinking anomaly over the WNP and the ascending anomaly over the equatorial eastern Pacific and western Indian Ocean, respectively. As a result, in the La Niña-like warming pattern easterly anomalies are present over the tropical WNP together with an anomalous cyclonic circulation from the SCS to the East China Sea, while in the El Niño-like warming pattern an anomalous cyclonic circulation is located over the central-eastern Pacific and an anomalous anticyclonic circulation appears in the upper troposphere over the WNP.

The responses in velocity potential and the associated divergent wind at 850 hPa (Figs. 4a and 4b) display nearly opposite distributions to those at 200 hPa. In the El Niño-like warming pattern, the low-level convergence over the equatorial eastern Pacific is stronger than that over the Atlantic, while the upper-level divergence over the former is weaker than that over the latter. This may be associated with the relatively warmer mean SST, which favors deeper convection, over the NA than over the equatorial eastern Pacific. The difference in low-level

©2020 American Geophysical Union. All rights reserved.

convergence between the tropical eastern Pacific and the tropical Atlantic leads to distinct circulation anomalies over the NA in response to the two warming patterns, namely changing from an anomalous cyclonic circulation to an anomalous anticyclonic circulation. The geographical distribution of the simulated positive/negative precipitation anomalies (Figs. 4e and 4f) agrees well with that expected from the ascending/descending anomalies except over the East Indian Ocean and the SCS, and is also consistent with the local maximum/minimum in SST anomalies (Fig. 1).

Finally, the LN87 model, which regards the boundary layer winds as a response to the underlying SST gradient in the tropics, is used to calculate the low-level winds induced by the difference in SST gradient between the two distinct warming patterns. The boundary layer winds derived from the LN87 model (Supplementary Fig. S6) show a distribution similar to the LLWs in responses to the two warming patterns (Figs. 3a and 3b). This strongly suggests that it is the difference in SST anomaly patterns between the two distinct warming patterns that is responsible for the difference in the spatial distribution and intensity of anomalies in tropical heating, and thus the anomalous tropical precipitation and the associated Walker circulation. These result in large anomalies in large-scale dynamic and thermodynamic conditions over the WNP and the NA, leading to large differences in TCTD in the two basins between the two warming patterns.

4. Conclusions and Discussion

Most previous studies have emphasized future changes in TC activity in response to an El Niño-like warming climate. Recent studies based on observations have documented a La Niña-like warming trend in the last decades. In this study, we have compared the responses of TCTD over the WNP and NA to the two distinct SST warming patterns. We found that the La Niña-like warming pattern tends to reduce TCTD over the WNP except over the SCS and along

©2020 American Geophysical Union. All rights reserved.

China coast, but increase TCTD over the NA, while the El Niño-like warming pattern generally reduces TC genesis and TCTD in most regions of both basins. Moreover, the different responses are primarily attributed to the different zonal SST gradients in the tropics, which trigger different distribution and intensity in tropical heating and the associated Walker circulation, resulting in large anomalies in large-scale dynamic and thermodynamic conditions over the WNP and the NA. These eventually lead to the different responses in TCTD in both basins to the two warming patterns.

An interesting issue is how sensitive the above results are to the amplitude of warming. To address the issue, we compared the responses of the boundary layer winds to the El Niño-like warming patterns for the periods of 2006–2099 (as the strong warming, Fig. 1b) and 2045–2099 (as the weak warming, Fig. S1) based on the LN87 model. In general, the response to the weak warming (Fig. S6c) displays a consistent spatial distribution with that to the strong warming (Fig. S6b), although the amplitude of the response is weaker as expected. More refined analyses will be detailed in our future studies.

It should be pointed out that the results from this study may be strongly affected by the simulation skill of the HIRAM-C180. Our model only focuses on the impacts of SST warming pattern, and does not consider other forcing associated with greenhouse gas changes. In fact, the change in atmospheric temperature due to changes in greenhouse gases may have important influences on TC activity as well, in addition to SST warming (Knutson et al., 2020), but it has not been included in the present study. We also noticed that our projected TC tracks over the NA in response to the El Niño-like warming are somewhat different from previous studies (e.g., Colbert et al., 2013; Murakami & Wang, 2010), despite the surface wind fields are similar to those evaluated using the LN87 model. Knutson et al. (2020) mentioned that it is difficult to identify a robust consensus projection for TC tracks. The present study does not resolve this issue either. However, this study does provide the consequence of another possible (La Niña-

©2020 American Geophysical Union. All rights reserved.

like) warming trend to TC activity over both the WNP and NA, although it is hard to determine whether future GW pattern is La Niña-like, El Niño-like or others. Therefore, results from this study can help better understand the potential future changes in TC activity and also call for attention to uncertainties in the projected future SST pattern when the impact of GW on TC activity is assessed. Further studies with improved multi−model simulations and accurate GW pattern considering consistent greenhouse gas change are required to reduce uncertainty in future TC projections.

Acknowledgments:

We are grateful to Prof. Li Tao and Dr. Lin Chen for their helps in conducting model experiments. This work has been supported by the National Natural Science Foundation of China (grants 41875114, 41775060, 41875057, and 41575052). Ruifen Zhan was supported in part by Open Research Fund of the State Key Laboratory of Severe Weather, Chinese Academy of Meteorological Sciences (2017Z017). The monthly ERSST v4 analyses were downloaded from https://www.esrl.noaa.gov/psd/data/gridded/data.noaa.ersst.v4.html. The HIRAM-C180 is downloaded from GFDL website https://www.gfdl.noaa.gov/hiram-quickstart/. The multi-model data of CMIP5 models are downloaded from http://data.ceda.ac.uk/badc/cmip5/data/cmip5. All the model simulation data required to reproduce the figures in the paper can be downloaded from the following DOI:10.6084/m9.figshare.11954511.

©2020 American Geophysical Union. All rights reserved.

Appendix

TC detection algorithm: The TC detection algorithm developed at the GFDL (https://www.gfdl.noaa.gov/tstorms/) was used to detect TCs in the simulations. First, the local minimum SLP center is searched by fitting a biquadratic to the SLP within a maximum distance of 3000 km. Second, if a closed contour with minimum SLP and maximum vorticity (greater than 1.5×10^{-4} s^{-1}) is found, the low-pressure system is counted as a storm center at that time. The tracker then tries to find as many closed contours about that low as it can find without going too far from the low center or running into contours claimed by another low. The maximum 10-m wind inside the closed contours is considered to be the maximum wind speed of the storm at that time. Third, the warm core represented by the maximum temperature anomaly (Ta; averaged between 500 hPa to 300 hPa representing the warm core) center is searched with a threshold of 1ºC. Ta should be no more than 1º latitude/longitude apart from the low center. Fourth, the storm center is connected to a track by taking a low center at time T-6h, extrapolating its motion forward to T+6h, and then looking for the storm within 750 km. Last, a TC is picked if the duration lasts at least 72 h for the detected low over the WNP and the NA with at least 24-h consecutive hours of warm core and maximum winds greater than 17 m s^{-1}.

The Lindzen-Nigam model: The linear steady-state one-layer boundary layer model that solves the surface winds given the SST distribution developed by Lindzen & Nigam (1987; LN87) includes the following equations:

$$\epsilon u' - f v' + \frac{A}{cos\theta}\frac{h'}{\partial\lambda} = \frac{B}{cos\theta}\frac{\partial T'}{\partial\lambda} \quad \text{(a)}$$

$$f u' + \epsilon v' + A\frac{\partial h'}{\partial\theta} - \frac{gn}{2R}\frac{\partial\bar{T}}{\partial\theta}h' = B\frac{\partial T'}{\partial\theta} \quad \text{(b)}$$

$$\frac{\partial u'}{\partial\lambda} + \frac{\partial(v'cos\theta)}{\partial\theta} + \frac{Rcos\theta}{\tau H_0}h' = 0 \quad \text{(c)}$$

where, λ is the longitude, θ is the latitude, $u'(v')$ is the zonal (meridional) wind averaged in

©2020 American Geophysical Union. All rights reserved.

the boundary layer, h' is the perturbation height at the top of the boundary layer (700 hPa), T' is the perturbation SST, g=9.8 m s^{-2} is gravity acceleration, the air density ρ=1.225kgm^{-3}, and the mean surface virtual temperature $\bar{T}$=288K, n=1/$\bar{T}$, γ=0.3 related to the static stability, the temperature lapse rate α=0.003Km^{-1}, the mean depth of boundary layer H_0=3 km, ϵ=2.5day^{-1} for the frictional coefficient in the boundary layer. R=6371 km for the radius of Earth, τ =30 min for the inverse relaxation time of the adjustment of the boundary layer height, the Coriolis parameter $f = 2\Omega sin\theta$ and Ω=7.272x$10^{-5}s^{-1}$, $A = \frac{g}{R}(2 - n\bar{T} + n\alpha H_0)$ and $B = \frac{gnH_0}{2R}(1 - \frac{2}{3}\gamma)$. The equations (a), (b) and (c) can be solved using a Fourier transform along longitude with finite difference method along latitude. Expanding *u'*, *v'* and *h'* as Fourier series, we can get

$$\epsilon u^m - f v^m + \frac{imA}{cos\theta}\frac{h^m}{\partial\lambda} = (\frac{B}{cos\theta}\frac{\partial T'}{\partial\lambda})^m \quad \text{(d)}$$

$$f u^m + \epsilon v^m + A\frac{\partial h^m}{\partial\theta} - \frac{gn}{2R}\frac{\partial\bar{T}}{\partial\theta}h^m = (B\frac{\partial T'}{\partial\theta})^m \quad \text{(e)}$$

$$imu^m + \frac{\partial(v^m cos\theta)}{\partial\theta} + \frac{Rcos\theta}{\tau H_0}h^m = 0 \quad \text{(f)}$$

where, *m* is the zonal wave number, $u'(\lambda,\theta) = \int_{-\propto}^{\propto} u^m(\theta)e^{im\lambda}$, $v'(\lambda,\theta) = \int_{-\propto}^{\propto} v^m(\theta)e^{im\lambda}$, and $h'(\lambda,\theta) = \int_{-\propto}^{\propto} h^m(\theta)e^{im\lambda}$. We used linear algebra to numerically solve (*u'*, *v'*, *h'*) with SST-forcing terms on the right-hand-side of the equations.

©2020 American Geophysical Union. All rights reserved.

References

Blake, E. S., Kimberlain, T. B., Berg, R. J., Cangialosi, J. P., & Beven III, J. L. (2013). Tropical Cyclone Report: Hurricane Sandy (AL182012). Tech. Rep. AL182012, NOAA/National Hurricane Center, 157 pp. [Available online at http://www.nhc.noaa.gov/data/tcr/AL182012_Sandy.pdf.]

Cai, W., Santoso, A., Wang, G., Yeh, S.-W., An, S.-I., Cobb, K. M., et al. (2015). ENSO and greenhouse warming. *Nature Climate Change*, *5*(9), 849–859. https://doi.org/10.1038/nclimate2743

Chen, L., Li, T., Yu, Y., & Behera, S. K. (2017). A possible explanation for the divergent projection of ENSO amplitude change under global warming. *Climate Dynamics*, *49*(11–12), 3799–3811. https://doi.org/10.1007/s00382-017-3544-x

Choi, J., Ham, Y., & McGregor, S. (2019). Atlantic-Pacific SST gradient change responsible for the weakening of North tropical Atlantic-ENSO relationship due to Global Warming. *Geophysical Research Letters*, *46*(13), 7574–7582. https://doi.org/10.1029/2019GL082804

Colbert, A. J., Soden, B. J., Vecchi, G. A., & Kirtman, B. P. (2013). The impact of anthropogenic climate change on North Atlantic tropical cyclone tracks. *Journal of Climate*, *26*(12), 4088–4095. https://doi.org/10.1175/JCLI-D-12-00342.1

Colbert, A. J., Soden, B. J., & Kirtman, B. P. (2015). The impact of natural and anthropogenic climate change on western North Pacific tropical cyclone tracks. *Journal of Climate*, *28*(5), 1806–1823. https://doi.org/10.1175/JCLI-D-14-00100.1

Compo, G. P., Whitaker, J. S., Sardeshmukh, P. D., Matsui, N., Allan, R. J., Yin, X., et al. (2011). The twentieth century reanalysis project. *Quarterly Journal of the Royal Meteorological Society*, *137*(654), 1–28. https://doi.org/10.1002/qj.776

Emanuel, K. A. (2013). Downscaling CMIP5 climate models shows increased tropical

Accepted Article

©2020 American Geophysical Union. All rights reserved.

cyclone activity over the 21st century. *Proceedings of the National Academy of Sciences*, *110*(30), 12219–12224. https://doi.org/10.1073/pnas.1301293110

Huang, B., Banzon, V. F., Freeman, E., Lawrimore, J., Liu, W., Peterson, T. C., et al. (2015). Extended reconstructed sea surface temperature version 4 (ERSST.v4). Part I: Upgrades and intercomparisons. *Journal of Climate*, *28*(3), 911–930. https://doi.org/10.1175/JCLI-D-14-00006.1

Knutson, T., Camargo, S. J., Chan, J. C. L., Emanuel, K., Ho, C.-H., Kossin, J., et al. (2019). Tropical cyclones and climate change assessment: Part I: Detection and attribution. *Bulletin of the American Meteorological Society*, *100*(10), 1987–2007. https://doi.org/10.1175/BAMS-D-18-0189.1

Knutson, T., Camargo, S. J., Chan, J. C. L., Emanuel, K., Ho, C.-H., Kossin, J., et al. (2020). Tropical cyclones and climate change assessment: Part II: Projected response to anthropogenic warming. *Bulletin of the American Meteorological Society*, https://doi.org/10.1175/BAMS-D-18-0194.1

Knutson, T. R., Sirutis, J. J., Garner, S. T., Vecchi, G. A., & Held, I. M. (2008). Simulated reduction in Atlantic hurricane frequency under twenty-first-century warming conditions. *Nature Geoscience*, *1*(6), 359–364. https://doi.org/10.1038/ngeo202

Knutson, T. R., Sirutis, J. J., Zhao, M., Tuleya, R. E., Bender, M., Vecchi, G. A., et al. (2015). Global projections of intense tropical cyclone activity for the late twenty-first century from dynamical downscaling of CMIP5/RCP4.5 scenarios. *Journal of Climate*, *28*(18), 7203–7224. https://doi.org/10.1175/JCLI-D-15-0129.1

Kohyama, T., Hartmann, D. L., & Battisti, D. S. (2017). La Niña–like mean-state response to global warming and potential oceanic roles. *Journal of Climate*, *30*(11), 4207–4225. https://doi.org/10.1175/JCLI-D-16-0441.1

Li, T., Kwon, M., Zhao, M., Kug, J.-S., Luo, J.-J., & Yu, W. (2010). Global warming shifts

Accepted Article

©2020 American Geophysical Union. All rights reserved.

Pacific tropical cyclone location. *Geophysical Research Letters*, *37*(21), L21804. https://doi.org/10.1029/2010GL045124

Lian, T., Chen, D., Ying, J., Huang, P., & Tang, Y. (2018). Tropical Pacific trends under global warming: El Niño-like or La Niña-like? *National Science Review*. https://doi.org/10.1093/nsr/nwy134

Lindzen, R. S., & Nigam, S. (1987). On the role of sea surface temperature gradients in forcing low-level winds and convergence in the tropics. *Journal of the Atmospheric Sciences*, *44*(17), 2418–2436. https://doi.org/10.1175/1520-0469(1987)044<2418:OTROSS>2.0.CO;2

Luo, J.-J., Wang, G., & Dommenget, D. (2018). May common model biases reduce CMIP5's ability to simulate the recent Pacific La Niña-like cooling? *Climate Dynamics*, *50*(3–4), 1335–1351. https://doi.org/10.1007/s00382-017-3688-8

Luo, J.-J., Sasaki, W., & Masumoto, Y. (2012). Indian Ocean warming modulates Pacific climate change. *Proceedings of the National Academy of Sciences*, *109*(46), 18701–18706. https://doi.org/10.1073/pnas.1210239109

Murakami, H., & Wang, B. (2010). Future change of North Atlantic tropical cyclone tracks: Projection by a 20-km-mesh global atmospheric model. *Journal of Climate*, *23*(10), 2699–2721. https://doi.org/10.1175/2010JCLI3338.1

Murakami, H., Wang, B., & Kitoh, A. (2011). Future change of western North Pacific typhoons: Projections by a 20-km-mesh global atmospheric model. *Journal of Climate*, *24*(4), 1154–1169. https://doi.org/10.1175/2010JCLI3723.1

Murakami, H., Wang, Y., Yoshimura, H., Mizuta, R., Sugi, M., Shindo, E., et al. (2012). Future changes in tropical cyclone activity projected by the new high-resolution MRI-AGCM. *Journal of Climate*, *25*(9), 3237–3260. https://doi.org/10.1175/JCLI-D-11-00415.1

Accepted Article

©2020 American Geophysical Union. All rights reserved.

Murakami, H., Villarini, G., Vecchi, G. A., Zhang, W., & Gudgel, R. (2016). Statistical–dynamical seasonal forecast of North Atlantic and U.S. landfalling tropical cyclones using the high-resolution GFDL FLOR coupled model. *Monthly Weather Review*, *144*(6), 2101–2123. https://doi.org/10.1175/MWR-D-15-0308.1

Nakamura, J., Camargo, S. J., Sobel, A. H., Henderson, N., Emanuel, K. A., Kumar, A., et al. (2017). Western North Pacific tropical cyclone model tracks in present and future climates. *Journal of Geophysical Research: Atmospheres*, *122*(18), 9721–9744. https://doi.org/10.1002/2017JD027007

Park, D.-S. R., Ho, C.-H., Chan, J. C. L., Ha, K.-J., Kim, H.-S., Kim, J., & Kim, J.-H. (2017). Asymmetric response of tropical cyclone activity to global warming over the North Atlantic and western North Pacific from CMIP5 model projections. *Scientific Reports*, *7*(1), 41354. https://doi.org/10.1038/srep41354

Patricola, C. M., Chang, P., & Saravanan, R. (2016). Degree of simulated suppression of Atlantic tropical cyclones modulated by flavour of El Niño. *Nature Geoscience*, *9*(2), 155–160. https://doi.org/10.1038/ngeo2624

Putman, W. M., & Lin, S.-J. (2007). Finite-volume transport on various cubed-sphere grids. *Journal of Computational Physics*, *227*(1), 55–78. https://doi.org/10.1016/j.jcp.2007.07.022

Schiermeier, Q. (2013). Did climate change cause typhoon Haiyan? *Nature*, 14139. https://doi.org/10.1038/nature.2013.14139

Seager, R., Cane, M., Henderson, N., Lee, D.-E., Abernathey, R., & Zhang, H. (2019). Strengthening tropical Pacific zonal sea surface temperature gradient consistent with rising greenhouse gases. *Nature Climate Change*, *9*(7), 517–522. https://doi.org/10.1038/s41558-019-0505-x

Sugi M, K. Yoshida and H. Murakami (2015), More tropical cyclone in a cooler climate?

©2020 American Geophysical Union. All rights reserved.

Geophys. Res. Lett., *42*,6780-6784, doi:10.1002/2015GL064929.

Taylor, K. E., Stouffer, R. J., & Meehl, G. A. (2012). An overview of CMIP5 and the experiment design. *Bulletin of the American Meteorological Society*, *93*(4), 485–498. https://doi.org/10.1175/BAMS-D-11-00094.1

Trenberth, K. E., Branstator, G. W., Karoly, D., Kumar, A., Lau, N.-C., & Ropelewski, C. (1998). Progress during TOGA in understanding and modeling global teleconnections associated with tropical sea surface temperatures. *Journal of Geophysical Research: Oceans*, *103*(C7), 14291–14324. https://doi.org/10.1029/97JC01444

Vecchi, G. A., Soden, B. J., Wittenberg, A. T., Held, I. M., Leetmaa, A., & Harrison, M. J. (2006). Weakening of tropical Pacific atmospheric circulation due to anthropogenic forcing. *Nature*, *441*(7089), 73–76. https://doi.org/10.1038/nature04744

Walsh, K. J. E., McBride, J. L., Klotzbach, P. J., Balachandran, S., Camargo, S. J., Holland, G., et al. (2016). Tropical cyclones and climate change. *Wiley Interdisciplinary Reviews: Climate Change*, *7*(1), 65–89. https://doi.org/10.1002/wcc.371

Wu, L., & Wang, B. (2004). Assessing impacts of global warming on tropical cyclone tracks. *Journal of Climate*, *17*(8), 1686–1698. https://doi.org/10.1175/1520-0442(2004)017<1686:AIOGWO>2.0.CO;2

Wu, L., & Chen, X. (2016). Revisiting the steering principal of tropical cyclone motion in a numerical experiment. *Atmospheric Chemistry and Physics*, *16*(23), 14925–14936. https://doi.org/10.5194/acp-16-14925-2016

Xie, S.-P., Deser, C., Vecchi, G. A., Ma, J., Teng, H., & Wittenberg, A. T. (2010). Global warming pattern formation: Sea surface temperature and rainfall. *J. Climate*, *23*(4), 966–986. https://doi:10.1175/2009JCLI3329.1.

Yokoi, S., Takayabu, Y. N., & Murakami, H. (2013). Attribution of projected future changes in tropical cyclone passage frequency over the western North Pacific. *Journal of*

Accepted Article

©2020 American Geophysical Union. All rights reserved.

Climate, *26*(12), 4096–4111. https://doi.org/10.1175/JCLI-D-12-00218.1

Zhang, C., & Wang, Y. (2017). Projected future changes of tropical cyclone activity over the Wwstern North and South Pacific in a 20-km-mesh regional climate model. *Journal of Climate*, *30*(15), 5923–5941. https://doi.org/10.1175/JCLI-D-16-0597.1

Zhang, L., & Li, T. (2014). A simple analytical model for understanding the formation of sea surface temperature patterns under global warming. *Journal of Climate*, *27*(22), 8413–8421. https://doi.org/10.1175/JCLI-D-14-00346.1

Zhao, M., Held, I. M., Lin, S.-J., & Vecchi, G. A. (2009). Simulations of global hurricane climatology, interannual variability, and response to global warming using a 50-km resolution GCM. *Journal of Climate*, *22*(24), 6653–6678. https://doi.org/10.1175/2009JCLI3049.1

Accepted Article

©2020 American Geophysical Union. All rights reserved.

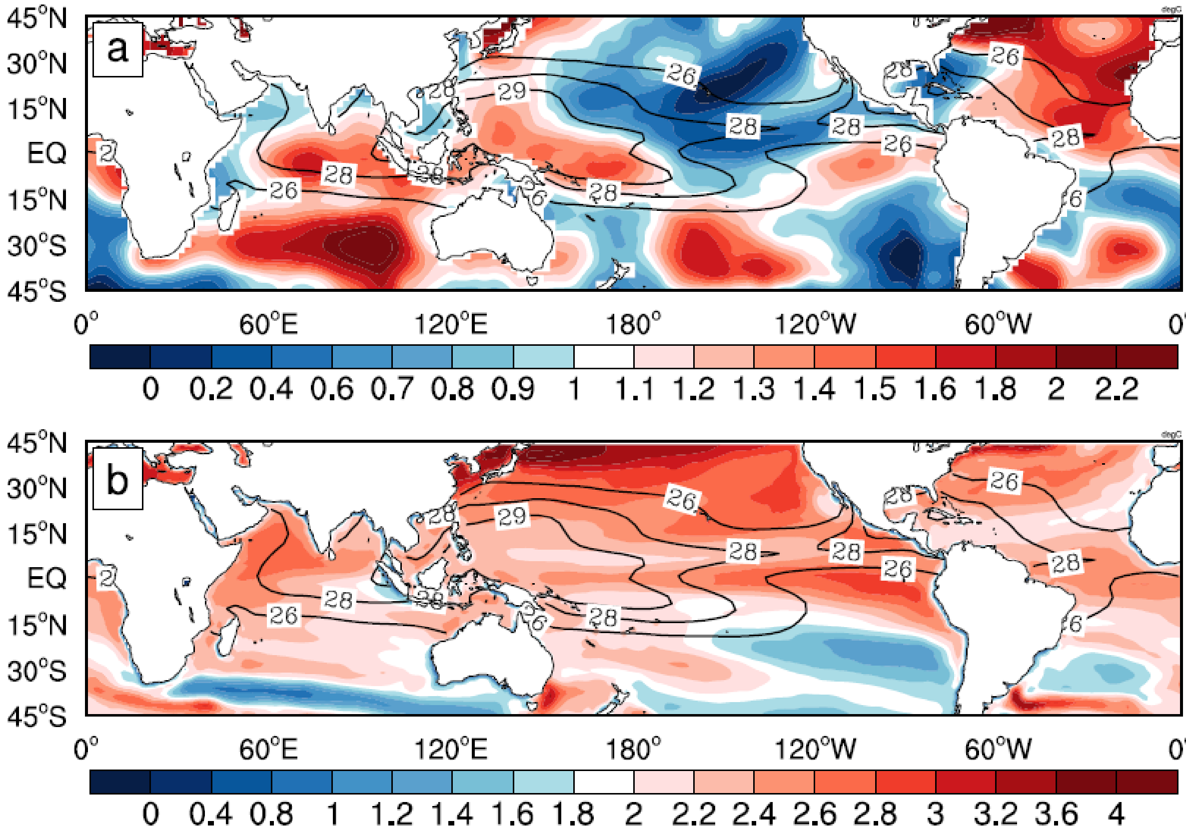

Figure 1. Linear trend increments of SST averaged in June-November (JJASON) from (a) observation during 1960–2014 and (b) ensemble mean of 12 CMIP5 model simulations during 2006–2099. The black contours represent the climatological JJASON mean SSTs in the CTRL run. The units of shading in (a) and (b) are °C in 55-years and °C in 94-years, respectively.

©2020 American Geophysical Union. All rights reserved.

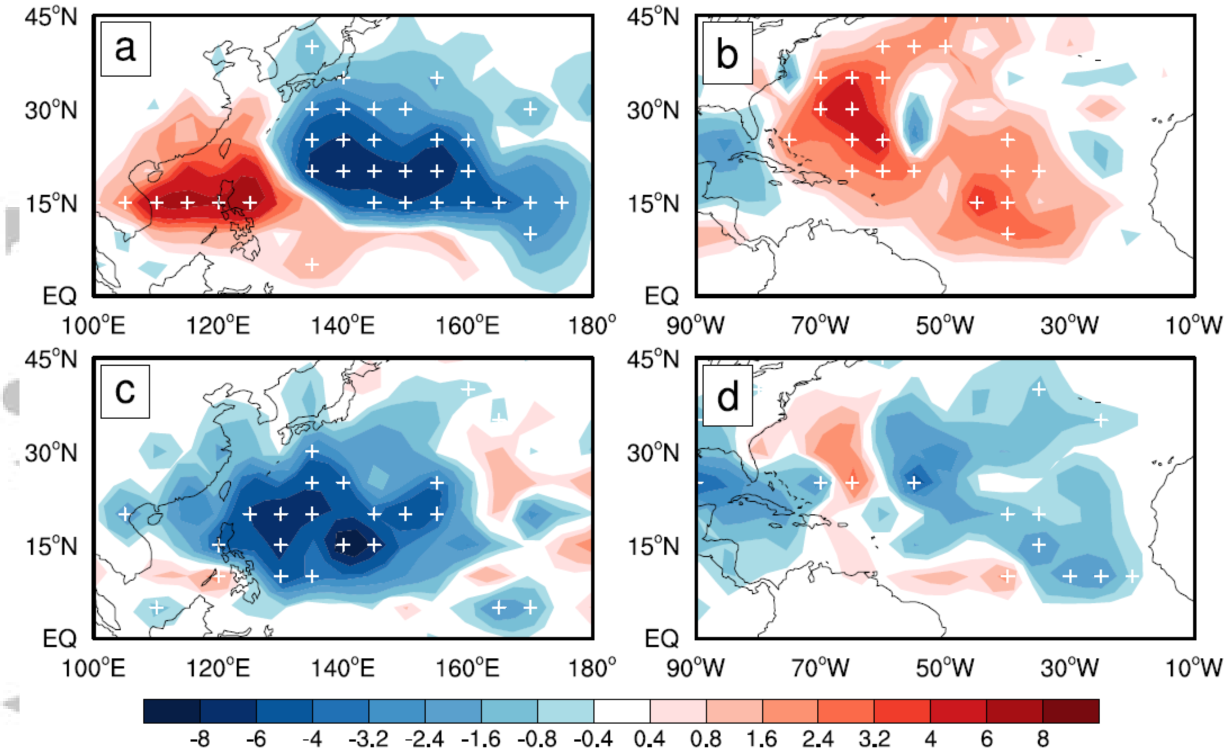

Figure 2. The simulated differences in TCTD averaged over June–November during 1990-2009 (a, b) between the GWLA and CTRL runs and (c, d) between the GWEL and CTRL runs over the WNP (left) and the NA (right), respectively. The white crosses represent area where the difference is statistically significant above 90% confidence level based on Student's t test.

Accepted

©2020 American Geophysical Union. All rights reserved.

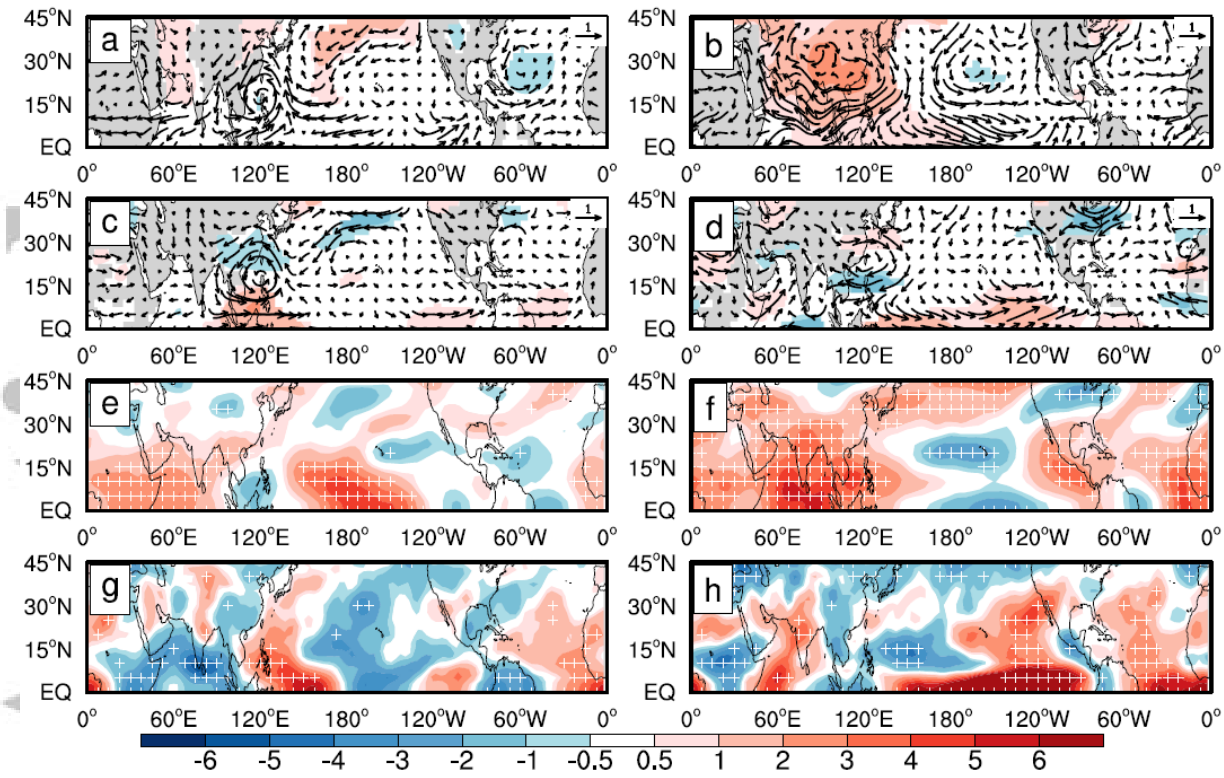

Figure 3. Changes in spatial patterns of (a, b) low-level winds (LLW in m s^{-1}; arrow) and sea level pressure (SLP in hPa; shaded), (c, d) steering flow (SF in m s^{-1}), (e, f) vertical zonal wind shear between 200 hPa and 850 hPa (VZWS in m s^{-1}), and (g, h) 600 hPa relative humidity (RH in g kg^{-1}) in response to the La Niña-like and El Niño-like warming patterns. The simulated differences were averaged over June–November during 1990–2009. (Left) The simulated differences between the GWLA and CTRL runs; (right) the differences between the GWEL and CTRL runs. The shading in (a-d) and white crosses in (e-h) represent areas where the difference is statistically significant above 90% confidence level based on Student's t test.

Accepted

©2020 American Geophysical Union. All rights reserved.

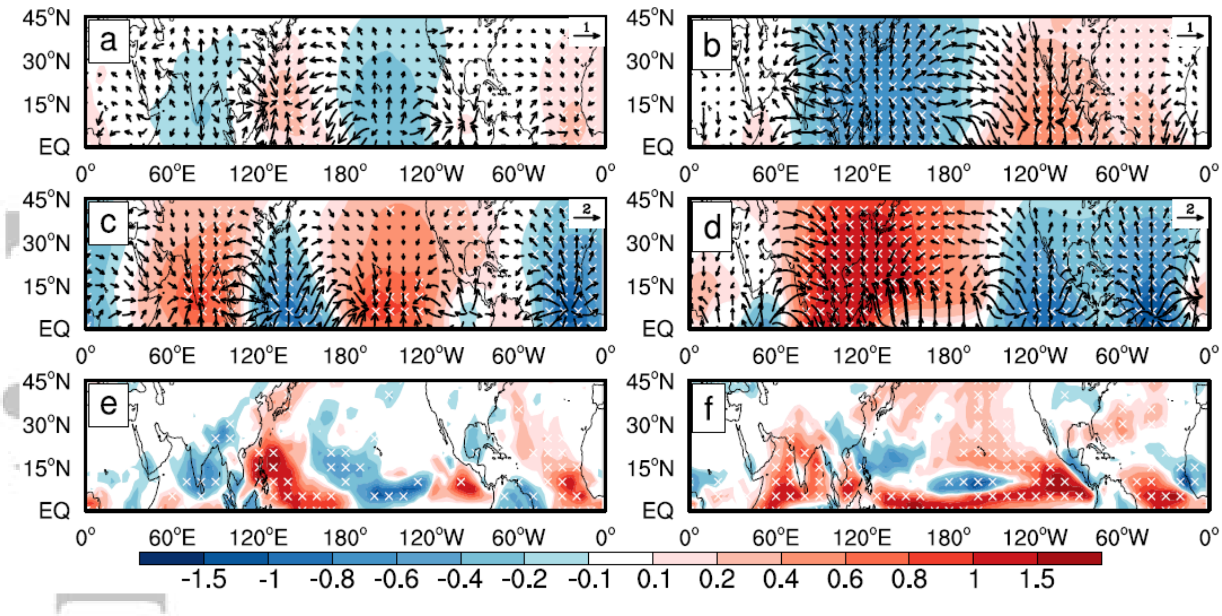

Figure 4. Changes in spatial patterns of velocity potential (VP in $10^6 m^2 s^{-1}$; shaded) and divergent wind ($m s^{-1}$; arrow) at (a-b) 850 hPa and (c-d) 200 hPa and (e-f) surface precipitation (Pr in $kg/m^2/day^{-1}$) in response to the La Niña-like and El Niño-like warming patterns. The simulated differences were averaged over June–November during 1990–2009. (Left) The simulated differences between the GWLA and CTRL runs; (right) the differences between the GWEL and CTRL runs. The white crosses in (a-f) represent areas where the difference is statistically significant above 90% confidence level based on Student's t test.

Accepted Article

©2020 American Geophysical Union. All rights reserved.